Research Article | Vol. 29, No. 11 / 24 May 2021 / Optics Express 17042
Optics EXPRESS

Numerical modeling of a hybrid hollow-core fiber for enhanced mid-infrared guidance

JULIANO G. HAYASHI,* SEYED M. A. MOUSAVI, ANDREA VENTURA, AND FRANCESCO POLETTI

Optoelectronics Research Centre, University of Southampton, Southampton, SO17 1BJ, UK
*jghayashi@outlook.com

Abstract: We propose a novel design of hollow-core fiber for enhanced light guidance in the mid-infrared. The structure combines an arrangement of non-touching antiresonant elements in the air core with a multilayer glass/polymer structure in the fiber's cladding. Through numerical modeling, we demonstrate that the combination of antiresonant/inhibited-coupling and photonic bandgap guidance mechanisms can decrease the optical loss of a tubular antiresonant fiber by more than one order of magnitude. More specifically, our simulations demonstrate losses of the HE_{11} mode in the few dB/km level, which can be tuned through mid-infrared wavelengths (5 µm-10.6 µm) by carefully optimizing the structural parameters of both structures. We also show that the hybrid hollow-core fiber design is more robust to bend-induced loss than an equivalent tubular antiresonant fiber or a Bragg/OmniGuide fiber. As a result, if successfully fabricated, the hybrid hollow-core fiber will offer low-loss, high beam-quality, effectively single-mode operation, and low bending losses, potentially solving many of the problems that affect all known mid-infrared fiber types.

1. Introduction

Hollow-core fibers have been the focus of much interest lately due to their ability to guide light in the air core rather than in a solid material. Such feature leads to reduced latency, reduced temperature sensitivity, ultra-low scattering, ultra-low loss, and low non-linearity, amongst others [1,2]. Over the years, different hollow-core optical fibers have been developed and successfully employed in many applications such as telecommunication, gas sensing, metrology, and high-power laser delivery. Examples of hollow-core waveguides are metal-coated fibers [3,4], Bragg/OmniGuide fibers [5–7], and Hollow-core Photonic Bandgap fibers [8,9]. Recently, antiresonant hollow-core fibers (AR-HCF) containing a core/cladding interface with inverted curvature, also known as negative curvature fibers, have received increasing attention due to their simple design and broadband operation [10–13].

For light guidance in the near-infrared, it has been shown that adding additional radial membranes/nested tubes in AR-HCFs helps reducing leakage loss [12,14], which dominates their overall loss. This can be done controllably with silica AR-HCFs, but becomes increasingly difficult to achieve for fibers made of MIR transmitting glasses, such as tellurite, chalcogenide, and fluoride. These glasses are more fragile than silica, have steeper viscosity by temperature curves, and are not commercially available as high-precision tubes. Therefore, up to now, only tubular AR structures with one ring of tubes in the air core have been fabricated [15–18]. If AR-HCFs are made of MIR glasses with losses of 0.1-10 dB/m, the glass absorption becomes negligible, and leakage loss dominates the fibers' overall loss.

In this work, we propose a different approach to reduce leakage loss in MIR AR-HCFs that does not require the employment of nested tubes [12] or conjoined elements [14]. Our novel

#423257 https://doi.org/10.1364/OE.423257
Journal © 2021 Received 23 Feb 2021; revised 10 Apr 2021; accepted 12 Apr 2021; published 19 May 2021

Optics EXPRESS

design combines a tubular antiresonant structure with a multilayer Bragg cladding. This hybrid fiber confines the light in the hollow-core simultaneously by antiresonant and photonic bandgap mechanisms. Both guidance mechanisms are very well known individually. However, to the best of our knowledge, no one has ever demonstrated that they can be combined effectively. Here, we show that this is possible and such combination can achieve a novel fiber design that incorporates the best properties of both worlds, namely the effective single-mode operation, the extremely low overlap of the fundamental optical mode with the cladding material, broadband operation, low non-linearity, high beam-quality and low straight and bending losses.

In Section 2, we discuss the selection of the structural parameters of both antiresonant and photonic bandgap structures to achieve enhanced guidance at a target wavelength band. In Section 3, we design a hybrid fiber to operate at the CO_2 laser emission line (10.6 µm) and numerically study its optical performance and bending losses. Modeling of equivalent tubular AR-HCF and Bragg/OmniGuide fibers is shown for comparison. In Section 4, we numerically demonstrate the hybrid fiber's wavelength tunability through the MIR, showing different hybrid fibers with enhanced guidance for wavelength operation going from 5 µm to 10.6 µm.

2. Hybrid hollow-core fiber design

Our proposed hybrid hollow-core fiber design combines an antiresonant structure in the air core with a multilayer Bragg structure in the fiber's jacket (Fig. 1). The light coupled in the core is confined simultaneously by antiresonant/inhibited-coupling and photonic bandgap guidance mechanisms. The antiresonant structure can be formed by any type of antiresonant elements, *e.g.*, circular non-touching capillaries [19], touching capillaries [20], conjugated elements [14], ice-cream cone shape elements [21], or nested elements [12,22]. Similarly, the Bragg cladding can be formed by a multilayer structure composed of two dielectric materials with different refractive index, such as glass/polymer [5–7], undoped/doped glass, or glass/air layers created by spacers [23] or rings of concentric air holes [24]. To illustrate the concept, we study systematically throughout this paper a hybrid fiber composed of six circular non-touching antiresonant tubes and a multilayer structure made of chalcogenide glass (IG3 - $Ge_{30}As_{13}Se_{32}Te_{25}$) [25] and FEP (Fluorinated Ethylene Propylene) polymer [26], as seen in Fig. 1. The IG3 glass was selected because it is a commercially available glass with low enough attenuation through the MIR [27], being smaller than 10 dB/m between 5 µm to 11 µm wavelength, and because of its co-drawing compatibility with the FEP polymer [18,27]. The experimental bulk losses of both materials measured in Ref. [27] are shown in Section 4.

The structural parameters in the hybrid design are chosen to overlap one transmission band of each guidance mechanism at the target operational wavelength (λ). For the tubular antiresonant structure, their characteristic transmission bands are defined as the regions between two consecutive resonant wavelengths (λ_m), which can be calculated by the ARROW model (Eq. (1)) [10],

$$\lambda_m = \frac{2\,.\,t_{tube}}{m}\,.\,\sqrt{n_g^2 - 1}, \tag{1}$$

where t_{tube} is the thickness of the inner tubes, n_g is the refractive index of the glass, and m is an integer representing the order of resonance. From Eq. (1), for a certain glass, the membrane thickness of the tubes can be selected to match the center of the desired band with the target operational wavelength. For the multilayer Bragg structure, the position of the photonic bandgap must be tuned to be centered around the target λ by selecting the thickness of the glass and polymer layers (t_g and t_p), which can be calculated with an approximated quarter-wave condition (Eq. (2)) [24,28],

$$t_i = \frac{\lambda}{4}\cdot\frac{1}{\sqrt{n_i^2 - 1}}, \tag{2}$$

Optics EXPRESS

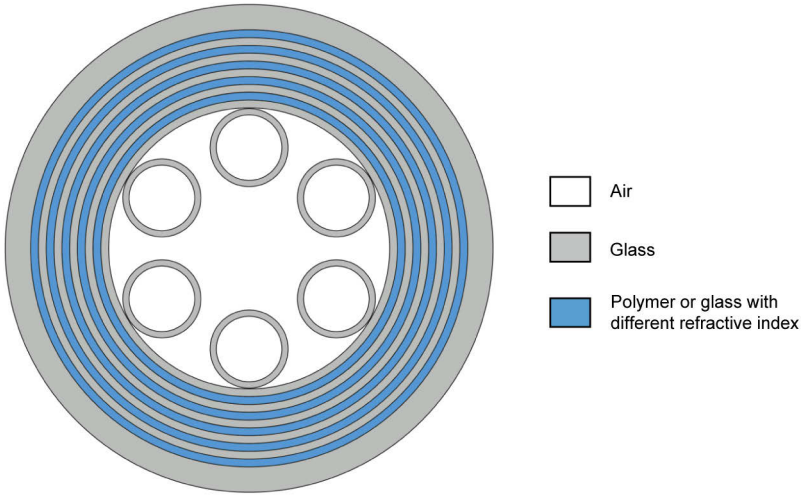

Fig. 1. Hybrid hollow-core fiber design combining a tubular antiresonant structure (six inner glass tubes) and a multilayer Bragg cladding. The dimensions of the multilayer structure are out of scale for better visualization.

where n_i is the refractive index of the respective material (glass or polymer) at the target λ. This expression considers the thickness of each layer equal to $\lambda/4$ and it is a reasonable approximation for the modes with an effective refractive index close to 1 [6], like the HE_{11} mode studied here. Apart from the tuning of the bandgap position according to the operational wavelength, the number of bilayers in the Bragg cladding must be carefully selected to guarantee a strong degree of confinement in the hollow-core. This confinement efficiency is strongly dependent on the refractive index contrast between the layers [6].

In the following sections, we numerically investigate the optical performance of the IG3/FEP hybrid fibers and compare it with equivalent tubular AR-HCF and Bragg fibers (same inner jacket diameter, constituent materials, thickness of the inner six tubes, number of bilayers, thicknesses of the layers). Using a finite element method modal solver in COMSOL multiphysics, we obtain the complex effective refractive index (n_{eff}) of the HE_{11} mode. The loss of the mode in dB/km (α) is calculated using

$$\alpha = \frac{40\,\pi \cdot \kappa}{\lambda \cdot ln(10)}, \tag{3}$$

where κ is the imaginary part of n_{eff} and λ is in km. All the modeling presented through this work specifically includes all the material losses, based on the experimental characterizations of the IG3 and FEP reported in [27]. The simulations were performed with extremely fine meshes with maximum size element of $\lambda/7$ and a high spatial resolution in the narrow regions. In the multilayer structure, mesh size elements smaller than half of the layer thickness were employed. Optimized perfectly matched layers (PMLs) were also used in their standard cylindrical definition to surround the simulation area, which enables the accurate calculation of confinement loss.

3. Hybrid hollow-core fiber for CO_2 laser delivery (10.6 µm)

To illustrate the concept and study in detail its properties, we designed a hybrid fiber for enhanced guidance at 10.6 µm wavelength (CO_2 laser line). Figure 2(a) shows the simulated optical loss of the HE_{11} mode for the IG3/FEP Hybrid fiber 1 (green curve). The Hybrid fiber 1 has six non-touching tubular elements in the core, 8 bilayers of FEP/IG3 in the cladding, and a core diameter (d_{core}) of 190 µm. For comparison, the losses of an equivalent Bragg fiber (black curve -

Optics EXPRESS

Bragg fiber 1) and an equivalent tubular AR-HCF (blue curve) are also plotted. These equivalent structures are identical to the Hybrid fiber 1, but without one of its guidance mechanism, *e.i.*, without the Bragg cladding (tubular AR-HCF 1) and without the inner tubular structure (Bragg fiber 1). Their schematics are shown in Fig. 2(b). The loss of a second Bragg fiber with d_{core}= 190 µm is also shown (red curve - Bragg fiber sc). All their structural parameters are listed in Table 1.

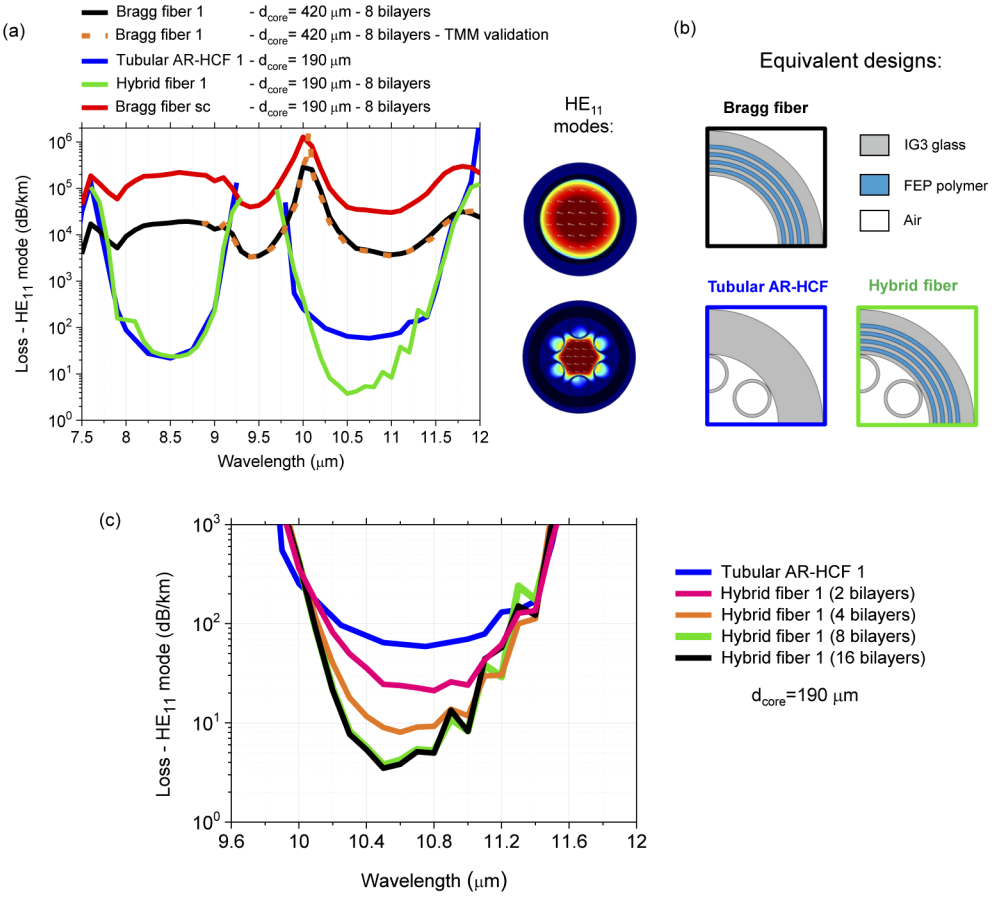

Fig. 2. (a) Simulated optical loss of the HE_{11} mode for the three fiber designs seen in (b). The modeling considers leakage and material losses, and the fibers have equivalent structural parameters, *i.e.*, same constituent materials (IG3/FEP), 8 bilayers, six tubular elements, same thicknesses of tubes and layers, and same inner jacket diameter (apart from Bragg fiber sc, which has an inner jacket diameter and core diameter of 190 µm). Insets: Example of the x-polarized HE_{11} modes in the Bragg and tubular/hybrid structure. (c) Loss of the Hybrid fiber 1 as a function of the number of bilayers in the Bragg structure.

At λ = 10.6 µm, the Hybrid fiber 1 exhibits a minimum optical loss of ~4 dB/km, which is three orders of magnitude smaller than the Bragg fiber 1 (~5000 dB/km) and one order of magnitude smaller than the tubular AR-HCF 1 (~60 dB/km). Such a degree of improvement in the light confinement is surprising. In the shorter wavelength transmission band around ~8.5 µm, the Hybrid fiber 1 exhibits losses similar to the tubular AR-HCF 1. At these wavelengths, the guided light is outside the photonic bandgap of the cladding's Bragg structure. As mentioned previously, the hybrid structure's enhanced guidance can be tuned through out the MIR by adjusting the wall thickness of the antiresonant elements and the thickness of the glass/polymer layers. In Section

Optics EXPRESS

Table 1. Structural parameters of the simulated fibers seen in Fig. 2 and Fig. 3.

	Bragg fiber 1	Bragg fiber sc	Tubular AR-HCF 1	Hybrid fiber 1
Core diameter	420 µm	190 µm	190 µm	190 µm
Inner jacket diameter	420 µm	190 µm	420 µm	420 µm
n°of inner glass tubes	0	0	6	6
Diameter of the inner tubes	0	0	115 µm	115 µm
Thickness of the inner tubes	0	0	7.5 µm	7.5 µm
Gap between the inner tubes	0	0	37.5 µm	37.5 µm
Number of bilayers	8	8	0	8
Glass layer thickness	1.02 µm	1.02 µm	0	1.02 µm
Polymer layer thickness	2.38 µm	2.38 µm	0	2.38 µm
Materials	IG3/FEP	IG3/FEP	IG3	IG3/FEP

4, we investigate the performance of a set of different hybrid fibers with operation wavelength varying from 5 µm to 10.6 µm.

It is well-known from the literature that the Bragg structure confinement's strength is strictly related to the refractive index contrast between the selected materials and the number of bilayers [6]. Figure 2(c) shows the HE_{11} loss of the Hybrid fiber 1 for varying the number of bilayers in the cladding (2, 4, 8 and 16). Interestingly, due to the high index contrast between IG3/FEP (2.8/1.32), 4 bilayers are sufficient to bring the minimum loss below 10 dB/km at $\lambda = 10.6$ µm (orange curve). In addition, the hybrid structure with 16 bilayers exhibits a minimum loss of ~ 4 dB/km (black curve), which is practically the same as the 8 bilayers case, indicating that the fabrication of more than 8 bilayers is redundant in this particular case, and if the bending loss is not concerned. For other wavelength operation or material combination, similar numerical modelling must be done to evaluate the number of bilayers required because their confinement efficiency varies according to the refractive index and absorption of the materials. At 10.9 µm, the Hybrid fiber 1 with 16 bilayers exhibits a loss ~ 2 dB/km higher than the 8-bilayers fiber. This difference is probably caused by the employment of slightly different mesh size in their Bragg claddings.

Note that the loss of the Bragg fiber 1 seen in Fig. 2(a) does not represent the minimum loss achievable for the HE_{11} mode in this type of the waveguide at $\lambda = 10.6$ µm. It is only a comparative case to illustrate the guidance improvement caused by the addition of a tubular antiresonant structure in its air core. According to the literature [28,29], an optimized Bragg fiber with 20 bilayers, $d_{core} = 500$ µm, and made of a chalcogenide glass and polymer with refractive indices similar to IG3/FEP, can achieve HE_{11} losses around 200 dB/km at λ=10.6 µm. This loss value is $\sim 3x$ and $\sim 50x$ larger in dB-scale than the losses seen for the tubular AR-HCF fiber 1 and the Hybrid fiber 1 (8 bilayers), respectively. However, this optimized Bragg fiber has a larger core diameter (500 µm), resulting also in a larger number of high-order modes and larger bending losses as will be shown below. In addition, the lowest-loss mode in Bragg fibers is the TE_{01} [6], which is more cumbersome to uniquely excite and collect than the HE_{11} mode (lowest-loss mode of the hybrid and tubular AR-HCFs).

The modelling of the Bragg fibers were validated with another set of simulations using transfer matrix method (TMM). As seen in Fig. 2(a), the loss of Bragg fiber 1 done with COMSOL (black curve) is good agreement with the loss calculate with TMM (dotted orange curve).

3.1. Bending loss

The bending loss of a fiber is a critical feature when the laser-delivery application requires bending of the waveguide around corners. Thus, numerical modeling was also performed to

Optics EXPRESS

evaluate the hybrid design's resilience to bending in comparison to an equivalent Bragg and tubular fibers. We employed the standard conformal transformation (Eq. (4)) to calculate their macro bending loss, which modifies the refractive index of an equivalent straight fiber to emulate the bending effect [12,30]. In Eq. (4), the R_c is the radius of curvature in the xz plane, x is the distance from the center of the waveguide, and n is the refractive index of the material (Fig. 3 inset). This approach does not consider the elasto-optic effect, which changes the refractive indices of the materials due to mechanical stress. Such approximation is widely employed in hollow-core fibers [12] because most of the light is guided in air.

$$n_i' = n_i.e^{\left(\frac{x}{R_c}\right)} \approx n_i.\left(1 + \frac{x}{R_c}\right). \tag{4}$$

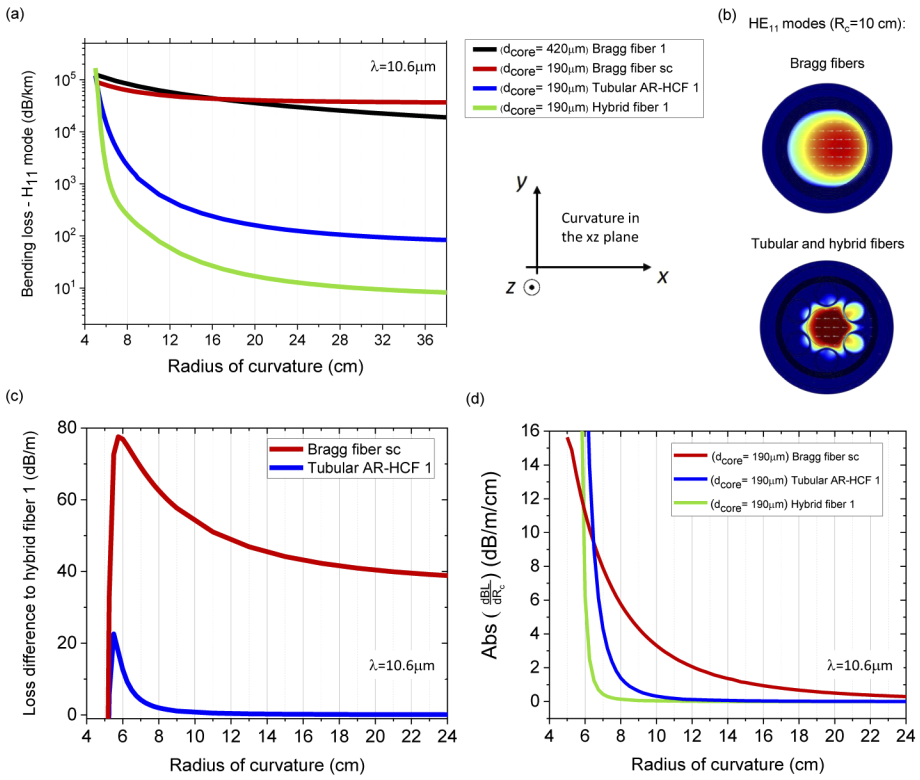

Fig. 3. (a) Overall loss of the HE_{11} mode when the fiber is bent as a function of R_c for the Bragg fibers (1 and sc), tubular AR-HCF 1, and Hybrid fiber 1. All Bragg structures have 8 bilayers of IG3/FEP. The curvature is restricted to the zx plane, the modes are polarized in the x direction, and λ=10.6 μm. The structural parameters of the fibers are listed in Table 1. (b) Power flow of the HE_{11} modes in the z direction for the different structures. (c) The difference in the loss between the fibers and the Hybrid fiber 1 as a function of R_c. (d) Comparison between the absolute value of $\frac{dBL}{dR_c}$ for the different designs.

Figure 3(a) shows the overall loss of the HE_{11} mode for the three studied designs as a function of the radius of curvature (at λ=10.6 μm). The conformal transformation used emulates a curvature in the zx plane (Fig. 3(a) inset), and an example of the modes at R_c=10 cm can be seen in Fig. 3(b). A second Bragg fiber with a core diameter identical to the Hybrid fiber 1 and tubular AR-HCF 1 is also investigated (Bragg fiber sc - red curve). According to the Fig. 3(a), for R_c=15 cm, the Hybrid fiber 1 (8 bilayers) exhibit an optical loss ~30 dB/km, being one order of magnitude

Optics EXPRESS

smaller than the tubular AR-HCF 1 (~270 dB/km) and three orders of magnitude smaller than both Bragg fibers (~46800 dB/km).

Figure 3(c) shows the difference of the HE_{11} loss between the Tubular AR-HCF 1 and the Hybrid fiber 1 (blue curve), and between the Bragg fiber sc and the Hybrid fiber 1 (red curve) when they are bent. In this plot, which is on a linear scale, it is more evident the difference in the bending performance between the designs. The Hybrid fiber 1 exhibits smaller losses to curvature as small as 5 cm in radius, and the difference is larger around $R_c \sim 5.65$ cm, being $\sim$ 80 dB/m and $\sim$ 22 dB/m compared to the Bragg fiber sc and tubular AR-HCF 1, respectively. Consequently, this result shows that the Hybrid fiber design has a significantly better optical performance when bent for R_c as small as 5 cm. Further optimization could be achieved by increasing the number of antiresonant elements inside the hollow-core, *e.g.*, employing a hybrid design with 8 inner capillaries. For $R_c < 5.25$ cm, the difference in loss becomes negative once the Hybrid fiber 1 becomes lossier than the other two designs. This occurs due to the increasing overlap of the mode with the FEP polymer in the hybrid fiber's cladding, which is lossier than the glass. The measured bulk loss of FEP and IG3 are $\sim 3 \cdot 10^4$ dB/m and $\sim$ 5.6 dB/m at $\lambda = 10.6\,\mu$m [27], respectively. However, in this particular case, the worse optical performance at $R_c < 5.25$ cm is irrelevant because the absolute value of the bending loss of all designs are larger than 50 dB/m. In this regime, all the three structures are not feasible for applications requiring such small bending of the waveguides. For $R_c > 10$ cm, the overall optical loss of the Hybrid fiber 1 considering leakage, material absorption, and bending, remains below 0.1 dB/m, which is a remarkable optical performance. If successfully fabricated, such fiber would unlock several laser delivery applications in the MIR.

The derivative of the overall HE_{11} mode loss of the fiber when bent ($\frac{dBL}{dR_c}$) as a function of the radius of curvature is also an interesting indicator of the fiber's resilience to bending. Figure 3(d) shows the absolute value of $\frac{dBL}{dR_c}$ from the three fiber designs with core diameter of 190 µm seen in Fig. 3(a). According to the plot, the guidance in the Hybrid fiber 1 is more robust to bending than the other designs. Its guidance of the HE_{11} is only perturbed at R_c smaller than 7 cm, while the tubular AR-HCF 1 and the Bragg fibers are considerably perturbed with R_c smaller than 10 cm and 20 cm, respectively.

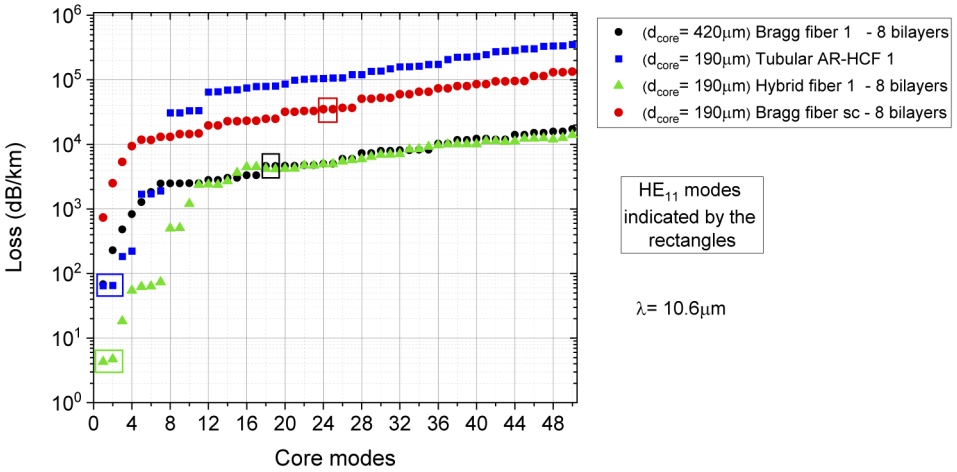

Fig. 4. Loss of the first 50 lowest-loss core modes in the Bragg fibers (sc and 1), tubular AR-HCF 1 and Hybrid fiber 1 at $\lambda = 10.6\,\mu$m. The HE_{11} modes of each fiber design are indicated by the coloured rectangles.

Optics EXPRESS

3.2. Modality

The hybrid fiber's modal characteristics are expected to be closer to its similar tubular AR-HCF than to those of the Bragg fibers. Figure 4 shows the simulated loss of the first 50 lowest-loss core (LLC) modes in the different designs and their respective HE_{11} modes highlighted by the coloured rectangles. According to Fig. 4, the Hybrid fiber 1 only guides effectively the LP_{01}, LP_{11} and LP_{21} mode groups (7 first LLC modes - green dots), once they have losses smaller than 0.1 dB/m. As indicated by the coloured rectangles, the HE_{11} modes have the lowest loss for both the tubular and hybrid structures. In contrast, the Bragg fiber 1 and sc have, at least, 17 and 23 core modes with loss smaller than their HE_{11} modes, respectively, and their lowest loss mode is the TE_{01}.

4. Tunability of the minimum loss window through the MIR

MIR applications such as gas sensing and laser delivery could benefit from low-loss hollow-core fibers with a good beam-quality, robust to bending, and with an operational wavelength in the 5 µm-10.6 µm window. As mentioned in Section 2, the enhanced guidance offered by the hybrid design can be tuned adjusting the thicknesses of the antiresonant tubes and the glass/polymer layers. To demonstrate such tunability potential, we designed a set of hybrid fibers to achieve enhanced guidance in each transmission band of our proposed tubular AR-HCF 1.

Figure 5 shows the simulated HE_{11} mode losses for this set of IG3/FEP hybrid fibers in the MIR. Each hybrid fiber has the same antiresonant structure of the tubular AR-HCF 1, but with a different Bragg structure with 20 bilayers matching one of the transmission windows of the antiresonant structure. The 20 bilayer Bragg structure was selected to ensure an optimized enhanced guidance for all the fibers. All structural parameters are listed in Table 2. The modeling of the fibers considers both leakage and material losses. For comparison, the bulk experimental losses of the FEP polymer and the IG3 glass measured in Ref. [27] are also shown.

Table 2. Structural parameters of the simulated fibers seen in Fig. 5.

	Tubular AR-HCF 1	Hybrid fiber 2	Hybrid fiber 3	Hybrid fiber 4	Hybrid fiber 5	Hybrid fiber 6
Core diameter	190 µm	190 µm	190 µm	190 µm	190 µm	190 µm
Inner jacket diameter	420 µm	420 µm	420 µm	420 µm	420 µm	420 µm
n°of inner glass tubes	6	6	6	6	6	6
Diameter of the inner tubes	115 µm	115 µm	115 µm	115 µm	115 µm	115 µm
Thickness of the inner tubes	7.5 µm	7.5 µm	7.5 µm	7.5 µm	7.5 µm	7.5 µm
Gap between the inner tubes	37.5 µm	37.5 µm	37.5 µm	37.5 µm	37.5 µm	37.5 µm
Number of bilayers	0	20	20	20	20	20
Glass layer thickness	0	0.48 µm	0.55 µm	0.66 µm	0.77 µm	1.02 µm
Polymer layer thickness	0	1.45 µm	1.68 µm	1.99 µm	2.33 µm	2.38 µm
Materials	IG3	IG3/FEP	IG3/FEP	IG3/FEP	IG3/FEP	IG3/FEP

According to Fig. 5, optical losses smaller than 1 dB/km and 5 dB/km could be achievable between λ= 5 µm - 7 µm and around λ= 10.6 µm, respectively. The combination of a large core diameter (190 µm) and a Bragg cladding with 20 bilayers leads to losses around 0.2 dB/km at $\lambda \sim$5.2 µm and 6 µm, 0.4 dB/km at $\lambda \sim$6.8 µm, and around 3 dB/km at $\lambda \sim$10.6 µm. For all wavelengths except between 7.7 µm - 9.5 µm, the Hybrid fiber 5 shows roughly an order of magnitude improvement in loss over the tubular AR-HCF 1. This is not observed between 7.7 µm - 9.5 µm because of the high attenuation of the FEP polymer in this region (black dashed-dotted curve). In addition, the abrupt variation of the FEP refractive index between λ= 7.2 µm - 9.5 µm (due to a resonance [27]) affects the cladding photonic bandgap. This problem could be solved

Optics EXPRESS

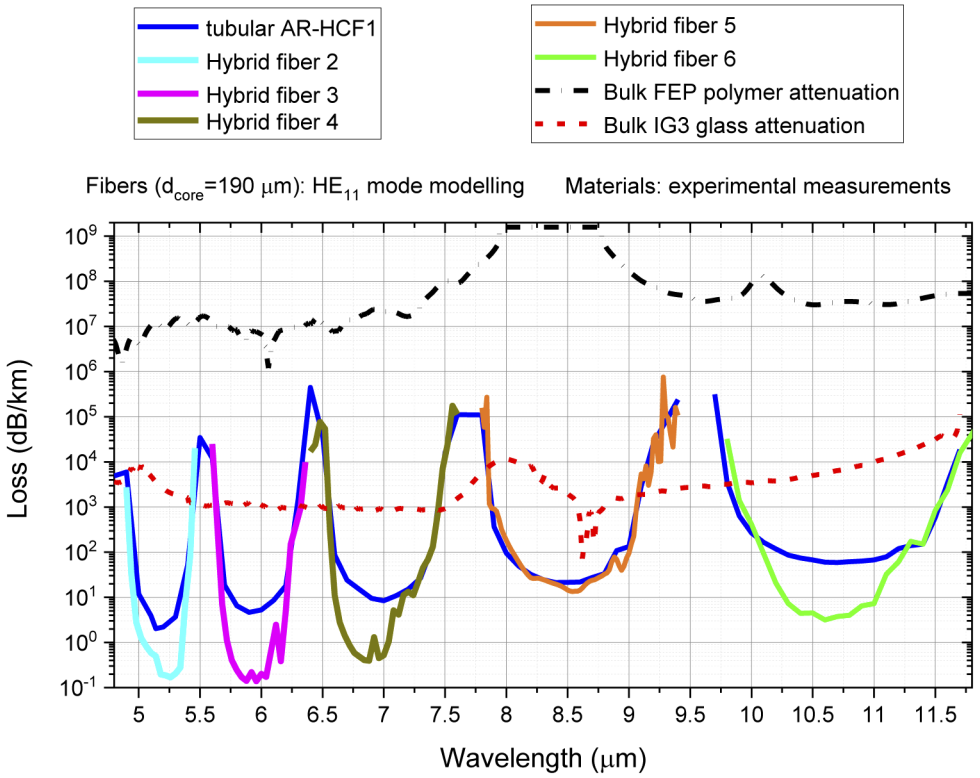

Fig. 5. Simulated optical loss of the HE_{11} mode for several Hybrid fibers designed to exhibit low-loss through the MIR (5 µm to 10.6 µm). Their structural parameters are the same as the tubular AR-HCF 1 (blue curve), but each IG3/FEP hybrid fiber has a different 20 bilayers Bragg cladding that individually matches one transmission band of the tubular structure. All structural parameters are listed in Table 2. The bulk experimental losses of the FEP polymer (black dashed-doted curve) and the IG3 glass (red dashed curve) are also shown.

by replacing the FEP polymer for another co-drawable thermoplastic with a resonance away from $\lambda \sim 8.5$ µm, leading to a hybrid fiber with enhanced guidance at such wavelength region. Defining the bandwidth as the transmission region with loss smaller than 1 dB/m (10^3 dB/km), Fig. 5 also shows that the Hybrid fibers have bandwidth of 0.53 µm (HF2), 0.66 µm (HF3), 0.89 µm (HF4), 1.18 µm (HF5) and 1.58 µm (HF6), respectively.

In a future fabrication attempt, deviations in the structural parameters of the drawn hybrid fiber could impact its guidance properties. Deviations in the thickness of the multilayers and in the thickness of the tubular membranes can lead to a partial mismatch of their respective transmission bands, reducing the bandwidth of the enhanced guidance. From Fig. 5, it is expected that such an issue will be less critical for longer operational wavelengths, where the enhanced guidance bandwidth is larger (1.58 µm for the Hybrid fiber 6). For the AR tubular structure, non-uniformities in the tubular membranes will increase the straight loss of the AR structure [18]. For the hybrid design, a further numerical study is required to quantify the overall impact of such non-uniformities in the straight and bending losses. The guidance capability of the Bragg structure could partially compensate the extra confinement loss of the AR structure.

Optics EXPRESS

5. Conclusion

We have proposed a novel design of hollow-core fiber combining a tubular antiresonant structure in the air core with a multilayer Bragg structure in the fiber's cladding. Through numerical modeling, we have demonstrated that the combination of antiresonant and photonic bandgap guidance mechanisms can decrease the optical loss of a tubular antiresonant fiber by more than one order of magnitude in the MIR (5 µm - 10.6 µm). The only exception where such a structure would not yield loss benefits is at those wavelengths where the polymer shows large absorption peaks.

For the hybrid fibers based on chalcogenide glass IG3 and FEP polymer, our simulations indicate that losses of the HE_{11} mode can be made smaller than a few dB/km, which can be tuned through MIR wavelengths by the redesigning of the structural parameters of both structures. More specifically, our modeling showed that IG3/FEP hybrid fibers can achieve minimum losses as small as 0.2 dB/km (λ = 5 µm - 6 µm), 0.4 dB/km (λ = 6.5 µm - 7.25 µm), and 3 dB/km (λ around 10.6 µm). A complementary study is required to understand if the optimization of both structures can further improve this remarkable optical performance, *e.g.*, replacing the number and shape of the antiresonant elements and/or employing a Bragg structure with varying layer thicknesses [28]. Bending loss study also demonstrated that the hybrid hollow-core fiber is more robust to bendings than an equivalent tubular antiresonant fiber and Bragg fiber.

Note that the level of confinement of a Bragg structure at the target wavelength is strictly related to the refractive index contrast between its constituents materials. Thus, we expect similar performances for hybrid fibers also made of other chalcogenides/thermoplastic materials. On the other hand, the hybrid design is unlikely to yield similarly good results for low index-contrast material combinations, *e.g.*, silica and doped silica, unless a few hundred of bilayers are employed in the fiber's cladding.

To conclude, by combining the best properties of the Bragg and antiresonant fibers, the hybrid structure is predicted to obtain remarkable performance in the MIR, theoretically better than those of any hollow-core fiber reported to date. They could offer low-loss (below a few dB/km), high beam-quality with an effectively single-mode operation and robust to bending down to ~ 10 cm radii. These features could unlock all the potential of MIR fiber-based technology in several fields, such as multispecies gas sensing, high-power/short pulse MIR laser delivery, gas-filled fiber lasers and nonlinear optics.

Funding. European Research Council (682724); Engineering and Physical Sciences Research Council (EP/N00762X/1, EP/P030181/1); Royal Society (NF170629).

Disclosures. The authors declare no conflicts of interest.

References

1. F. Poletti, N. Wheeler, M. Petrovich, N. Baddela, E. N. Fokoua, J. Hayes, D. Gray, Z. Li, R. Slavík, and D. Richardson, "Towards high-capacity fibre-optic communications at the speed of light in vacuum," Nat. Photonics **7**(4), 279–284 (2013).
2. E. N. Fokoua, M. N. Petrovich, T. Bradley, F. Poletti, D. J. Richardson, and R. Slavík, "How to make the propagation time through an optical fiber fully insensitive to temperature variations," Optica **4**(6), 659–668 (2017).
3. J. A. Harrington, "A review of IR transmitting, hollow waveguides," Fiber & Integr. Opt. **19**(3), 211–227 (2000).
4. J. M. Kriesel, N. Gat, B. E. Bernacki, R. L. Erikson, B. D. Cannon, T. L. Myers, C. M. Bledt, and J. A. Harrington, "Hollow core fiber optics for mid-wave and long-wave infrared spectroscopy," Proc. SPIE **8018**, 80180V (2011).
5. B. Temelkuran, S. D. Hart, G. Benoit, J. D. Joannopoulos, and Y. Fink, "Wavelength-scalable hollow optical fibres with large photonic bandgaps for CO_2 laser transmission," Nature **420**(6916), 650–653 (2002).
6. S. G. Johnson, M. Ibanescu, M. Skorobogatiy, O. Weisberg, T. D. Engeness, M. Soljačić, S. A. Jacobs, J. Joannopoulos, and Y. Fink, "Low-loss asymptotically single-mode propagation in large-core omniguide fibers," Opt. Express **9**(13), 748–779 (2001).
7. S. D. Hart, G. R. Maskaly, B. Temelkuran, P. H. Prideaux, J. D. Joannopoulos, and Y. Fink, "External reflection from omnidirectional dielectric mirror fibers," Science **296**(5567), 510–513 (2002).
8. F. Poletti, M. N. Petrovich, and D. J. Richardson, "Hollow-core photonic bandgap fibers: technology and applications," Nanophotonics **2**(5-6), 315–340 (2013).

Optics EXPRESS

9. F. Benabid, "Hollow-core photonic bandgap fibre: new light guidance for new science and technology," Phil. Trans. R. Soc. A. **364**(1849), 3439–3462 (2006).
10. F. Yu and J. C. Knight, "Negative curvature hollow-core optical fiber," IEEE J. Sel. Top. Quantum Electron. **22**(2), 146–155 (2016).
11. B. Debord, A. Amsanpally, M. Chafer, A. Baz, M. Maurel, J. Blondy, E. Hugonnot, F. Scol, L. Vincetti, F. Gérôme, and F. Benabid, "Ultralow transmission loss in inhibited-coupling guiding hollow fibers," Optica **4**(2), 209–217 (2017).
12. F. Poletti, "Nested antiresonant nodeless hollow core fiber," Opt. Express **22**(20), 23807–23828 (2014).
13. I. A. Bufetov, A. F. Kosolapov, A. D. Pryamikov, A. V. Gladyshev, A. N. Kolyadin, A. A. Krylov, Y. P. Yatsenko, and A. S. Biriukov, "Revolver hollow core optical fibers," Fibers **6**(2), 39 (2018).
14. S.-F. Gao, Y.-Y. Wang, W. Ding, D.-L. Jiang, S. Gu, X. Zhang, and P. Wang, "Hollow-core conjoined-tube negative-curvature fibre with ultralow loss," Nat. Commun. **9**(1), 2828 (2018).
15. A. F. Kosolapov, A. D. Pryamikov, A. S. Biriukov, V. S. Shiryaev, M. S. Astapovich, G. E. Snopatin, V. G. Plotnichenko, M. F. Churbanov, and E. M. Dianov, "Demonstration of CO_2-laser power delivery through chalcogenide-glass fiber with negative-curvature hollow core," Opt. Express **19**(25), 25723–25728 (2011).
16. R. R. Gattass, D. Rhonehouse, D. Gibson, C. C. McClain, R. Thapa, V. Q. Nguyen, S. S. Bayya, R. J. Weiblen, C. R. Menyuk, L. B. Shaw, and J. S. Sanghera, "Infrared glass-based negative-curvature anti-resonant fibers fabricated through extrusion," Opt. Express **24**(22), 25697–25703 (2016).
17. A. Ventura, J. G. Hayashi, J. Cimek, G. Jasion, P. Janicek, F. B. Slimen, N. White, Q. Fu, L. Xu, H. Sakr, N. V. Wheeler, D. J. Richardson, and F. Poletti, "Extruded tellurite antiresonant hollow core fiber for mid-IR operation," Opt. Express **28**(11), 16542–16553 (2020).
18. J. G. Hayashi, A. Ventura, G. T. Jasion, J. Cimek, F. B. Slimen, N. White, H. Sakr, N. V. Wheeler, and F. Poletti, "Extruded chalcogenide antiresonant hollow core fiber for mid-IR laser delivery," Proc. SPIE **11206**, 1–4 (2019).
19. A. N. Kolyadin, A. F. Kosolapov, A. D. Pryamikov, A. S. Biriukov, V. G. Plotnichenko, and E. M. Dianov, "Light transmission in negative curvature hollow core fiber in extremely high material loss region," Opt. Express **21**(8), 9514–9519 (2013).
20. A. D. Pryamikov, A. S. Biriukov, A. F. Kosolapov, V. G. Plotnichenko, S. L. Semjonov, and E. M. Dianov, "Demonstration of a waveguide regime for a silica hollow-core microstructured optical fiber with a negative curvature of the core boundary in the spectral region> 3.5 μm," Opt. Express **19**(2), 1441–1448 (2011).
21. F. Yu, W. J. Wadsworth, and J. C. Knight, "Low loss silica hollow core fibers for 3–4 μm spectral region," Opt. Express **20**(10), 11153–11158 (2012).
22. W. Belardi, "Design and properties of hollow antiresonant fibers for the visible and near infrared spectral range," J. Lightwave Technol. **33**(21), 4497–4503 (2015).
23. A. Dupuis, K. Stoeffler, B. Ung, C. Dubois, and M. Skorobogatiy, "Transmission measurements of hollow-core THz bragg fibers," J. Opt. Soc. Am. B **28**(4), 896–907 (2011).
24. A. Argyros, I. M. Bassett, M. A. van Eijkelenborg, and M. C. Large, "Analysis of ring-structured bragg fibres for single TE mode guidance," Opt. Express **12**(12), 2688–2698 (2004).
25. Vitron, "Vitron IG3 glass," https://www.vitron.de/files/VITRON_IG-3_Datenblatt_Jan_2015.pdf.
26. Du Pont, "FEP handbook," http://www.rjchase.com/fep_handbook.pdf.
27. A. Ventura, F. B. Slimen, J. Lousteau, N. White, A. Masoudi, P. Janicek, and F. Poletti, "Flexible mid-IR fiber bundle for thermal imaging of inaccessible areas," Opt. Express **27**(15), 20259–20272 (2019).
28. O. Weisberg, S. A. Jacobs, M. Skorobogatiy, S. G. Johnson, and U. Kolodny, "Photonic crystal waveguides and systems using such waveguides," (2007). US Patent 7, 231, 122.
29. Y. Fink, V. Fuflyigin, R. Ahmad, E. G. Anderson, B. Farnsworth, Y. Kahn, A. Micetich, P. Prideaux, and U. Kolodny, "Photonic crystal waveguides and systems using such waveguides," (2007). US Patent 7, 310, 466.
30. M. Heiblum and J. Harris, "Analysis of curved optical waveguides by conformal transformation," IEEE J. Quantum Electron. **11**(2), 75–83 (1975).